孙渊，李辉，陈智锋. 根土复合体在循环单剪条件下的响应行为及离散元模拟研究[J]. 水利水电技术(中英文)，2025，56(S1)：665-680.
SUN Yuan，LI Hui，CHENG Zhifeng. Cyclic behavior of root-loess composites under direct simple shear test conditions and insights from discrete element method modeling[J]. Water Resources and Hydropower Engineering，2025，56(S1)：665-680.

Cyclic behavior of root-loess composites under direct simple shear test conditions and insights from discrete element method modeling

SUN Yuan[1]，LI Hui[2]，CHENG Zhifeng[2]
(1. The First Construction Engineering Company of China Construction Third Engineering Bureau，Wuhan 430000，Hubei，China；
2. College of Civil Engineering，Qinghai University，Xining 810016，Qinghai，China)

Abstract：Plant roots are widely known to provide mechanical reinforcement to soils against shearing and further increase slope stability. However，whether roots provide reinforcement to loess cyclic re-sistance and how various factors affect roots reinforcement during seismic loading have rarely been studied. The objective is to conduct a series of cyclic direct simple shear tests and DEM numerical simulation to investigate the cyclic behaviour of rooted loess. The effects of initial static shear stress and loading frequency on the cyclic resistance of root-soil composites were first investigated. After that，cyclic direct simple shear simulations at constant volume were carried out based on the discrete element method (PFC^{3D}) to investigate the effects of root geome-try，mechanical traits and root-soil bond strength on the cyclic strength of rooted loess. It was discovered that the roots could effectively improve the cyclic resistance of loess. The cyclic resistance of the root-soil composite decreases with the increase of the initial shear stress，then increases，and improves with the increase of the frequency. The simulation result show that increases in root elastic modulus and root-soil interfacial bond strength can all enhance the cyclic resistance of root-soil composites，and the maximum cyclic resistance of the root-soil composite was obtained when the initial inclination angle of the root system was 90°.

Keywords：root-soil composite；cyclic direct simple shear tests；PFC^{3D}
DOI：10.13928/j.cnki.wrahe.2025.S1.100
中图分类号：TU444 **文献标志码**：A **文章编号**：1000-0860(2025)S1-0665-16

根土复合体在循环单剪条件下的响应行为及离散元模拟研究

孙 渊[1]，李 辉[2]，陈智锋[2]
(1. 中建三局第一建设工程有限责任公司，湖北 武汉 430000；
2. 青海大学 土木水利学院，青海 西宁 810016)

Article history：Received 20 Autumn 2024
收稿日期：2024-08-20
Financial Aid：Key Research，Development and Transformation Projects of Qinghai Science and Technology Department in Qinghai Province(No. 2022-SF-159)
基金项目：青海省科技厅科技成果转化专项项目(2022-SF-159)
About the author：SUN Yuan(1999—)，male，graduate student，mainly engaged in geotechnical engineering disaster prevention and mitigation research. E-mail：2823211781@qq.com
作者简介：孙 渊(1999—)，男，硕士研究生，主要从事岩土工程防灾减灾研究。E-mail：2823211781@qq.com
Corresponding author：LI Hui(1978—)，male，professor，doctoral degree，mainly engaged in geotechnical engineering disaster prevention and mitigation research. E-mail：lihui@qhu.edu.cn
通信作者：李 辉(1978—)，男，教授，博士，主要从事岩土工程防灾减灾研究。E-mail：lihui@qhu.edu.cn

摘　要：植被根系可以提高土体抵抗剪切的能力，抑制浅层滑坡。但是，根系是否可以增强黄土的循环抵抗能力，以及地震荷载下各种因素对根系力学加固效应的影响缺乏相关的研究。通过进行一系列动单剪试验和离散元模拟来探究加根黄土的循环行为。首先调查了初始静剪应力和加载频率对根土复合体试样循环抵抗能力的影响。之后基于离散元方法(PFC^{3D})，进行常体积循环直接简单剪切模拟，探究根系几何、力学特性及根土间胶结强度对加根黄土循环强度的影响。研究结果表明根系可以有效提高黄土的循环抵抗能力。根土复合体的循环抵抗能力随初始剪应力的增加先下降，后上升，随频率的增加不断提高。模拟结果表明根系弹性模量、根土间胶结强度的增加均可以提升根土复合体的循环抵抗能力。当根系的初始倾斜角度为90°时，根土复合体的循环抵抗能力获得最大值。

关键词：根土复合体；动态循环单剪；PFC^{3D}

1 Introduction

The vegetation roots grow and extend downward in the soil (up to 2 m deep most), forming a root-soil composite, in nearly all cases with more than 50% of roots being found in the top 0.3 m of soil[1]. The main types of root architectures are: heartroot, taproot, and plateroot systems. The presence of vegetation on slopes not only provides ecological benefits, but is also widely believed to suppress shallow landslides[2-4]. Shallow landslides constitute one of the most hazardous categories of mass movements[5], posing a huge threat to the safety of human life, property and infrastructure. In recent years, ecological slope protection technology which can promote carbon-neutral development has been successfully applied in a wide range of projects, such as: highway slope, cover slope of a solid waste landfill, streambank reinforcement[6], etc.

Plant affects the soil properties of slopes mainly through mechanical and hydrological processes. Due to the different response of roots and soil to stress[7], stresses in the soil under loading are transferred to the roots in a manner that is alike to the reinforcement of concrete structures by steel or fiberglass, thus producing mechanical reinforcement. Root-soil composites resist shear primarily by mobilizing tensile deformation of the root system and friction at the root-soil interface. On the other hand, the radial expansion of the roots increases the contact stress between soil particles, thus increasing the densification of the soil around the roots[8-9]. The mucus secreted by the roots glues the soil particles around the roots, directly increasing the cohesion and structural stability of the soil[10]. The magnitude of root reinforcement is related to many factors: root distribution density, tensile strength, tensile modulus, root length, alignment angularity/straightness of the roots, orientation of the roots relative to the direction of shear plane, root architecture, vegetation species, root-soil bond strength, soil moisture content, normal pressure, and has a high degree of spatial and temporal variability. Accurately predicting the mechanical reinforcement of the roots remains a challenge due to the complexity of root-soil interactions and the stochastic variability in the properties of both. Plant roots also regulate the hydrological conditions around the roots, transferring water from wet sites to dry soils, and the moisture content of soils closer to the root system is lower[11]. Aboveground stems and leaves of vegetation intercept rainfall[12], which in combination with evapotranspiration reduces the water content of slopes, changes matrix suction, and delays soils from reaching critical saturation levels. At present, a large number of scholars have studied the reinforcing effect of root-soil composites in terms of macroscopic mechanical properties, including in-situ tests and laboratory tests using live roots and roots analogues[13]. However these studies have concentrated on roots reinforcement in monotonic stress path, such as compression、extension、direct or simple shear stress path. In addition to these experimental studies, many mechanical models for quantifying soil reinforcement have been established on the basis of a simplified consideration of the main influencing factors[14-20].

Regarding the cyclic behaviour of root soil composite, very limited investigation on the element behaviour can be found in the literature to the best of our knowledge. LIANG et al[21] fabricate root analogues using 3D printing techniques, and conducted a series of rooted slope centrifuge tests. It is concluded that roots may be

an effective seismic slope stabilization method for slopes of smaller height. KARIMZADEH et al[22] concluded by conducting undrained triaxial tests that the roots can effectively increase the liquefaction resistance of sand and change the failure mechanism from limited flow to cyclic mobility. However, in the context of the widespread application of ecological slope protection technology, the slope protection potential of vegetation roots in loess areas under seismic action has no experimental justification in terms of relevant dynamic properties and a clear underlying mechanism. The effects of initial static shear stress and cyclic shear frequency on cyclic resistance of root-soil composites has received relatively little attention. Under seismic loading, the root-soil composite unit in ecological slope engineering will be subjected to the loading conditions of initial static shear stress action and rotation of the principal stress axis, resulting in simple shear-dominated deformation. Cyclic direct simple shear tests (CDSS) can more realistically reproduce the stress state of a soil unit under seismic loading[23-24] and can more accurately measure volumetric strains compared to the dynamic triaxial test (CTX). Many scholars have now conducted monotonic and cyclic direct simple shear tests under the influence of different factors (density, overburden pressure, initial static shear stress, frequency, shear strain amplitude, and volume change boundary conditions[25]) on sandy soils[26], rubber-sand mixture[27], loess[28], and clays[29]. EIGhoraibye et al[30] concluded from CDSS tests on Ottawa F65 sand that under undrained cyclic shear conditions, the secant shear modulus decreases with continuous application of shear stress, while the damping ratio first rises, then plateaus, and finally decreases. Past studies on the effect of initial shear stress on cyclic resistance have not reached a consistent conclusion, which can show different patterns such as decreasing[31-32], increasing first and then decreasing[33-34], probably be due to the fact that it can be influenced by a combination of factors such as relative density, confining pressure, and soil properties[35]. PARK et al[36] conducted that the cyclic resistance of loose sands decreases continuously with increasing initial shear stress, while that of dense sands does not necessarily decrease, which is influenced by the combination of consolidation pressure and initial shear stress.

Due to the complexity and variability of roots geometrical and mechanical traits, it is difficult to prepare completely identical specimens in the test, thus numerical simulation methods become a promising alternative. The finite element method was first used for the simulation of three-dimensional direct shear tests of root-soil composites[37-38], but it encounters mesh-induced convergence problems at larger strains in the soil. The discrete element method was first developed by CUNDALL et al[39] and has been widely used in geotechnical engineering[40-41]. Particle flow software (PFC^{3D}) modeling can obtain a large amount of microscopic contact information, such as local stress-strain, pore size distribution, strong force chain evolution, bonding damage, and complex and comprehensive interactions between soil particles, thus revealing the potential microscopic mechanisms under the macroscopic response. Many scholars have performed simple shear simulations, and investigated the changes in force chain, principal stress direction, non-coaxiality, fabric structure anisotropy, stress-strain distribution inhomogeneity, coordination number, and pore distribution during shear under the influence of various factors, such as instrument type, initial porosity ratio, particle-to-sample size ratio, and base type, etc[42-49]. BOURRIER et al[50] established a numerical model of direct shear tests of rooted granular soils based on the DEM, and explored the effects of the root mechanical traits, root-soil interfacial friction angle and of the root number for the different soil types. DEM simulations have been shown to reasonably reproduce the cyclic response of granular materials[51-53], making them an appropriate tool for exploring the cyclic response of bonded reinforcement materials from a microscopic point of view. However, no studies have yet conducted to simulate dynamic element tests of root soil composite with discrete element method. On the other hand, PFC^{3D} can customize the contact relationship between particles as a way to meet model-specific needs. MA et al[54] defined a displacement-softening contact model that solves the problem of material tensile to compressive strength ratios that do not match the experimental results. JIANG et al[55] developed a contact model that considers torsional and rotational resistance

forces, which can well capture the mechanical behavior of sand in direct shear. Therefore, a more appropriate customized contact relationship is used for the simulation of loess in this paper.

This article investigates the cyclic behavior of root-soil composites from a macro-micro scale perspective by means of stress-controlled constant volume cyclic direct simple shear tests and DEM numerical simulations, to provide information for establishing analytical soil reinforcement dynamic model. The paper has been organized in the following way. Firstly, a series of cyclic simple shear test results for rooted and non-rooted loess under different initial static shear stresses and frequencies are presented. Then, the evolution laws of force chains, principal stresses direction, the fabric, non-coaxial angles and stress inhomogeneities for root-soil composites in shear simulations are shown. The numerical results also allowed analyzing the influence of root-soil interfacial shear strength, roots mechanical and geometrical property to soil reinforcement by roots.

2 Materials and Methods

2.1 *Study area and plant*

The study area is located in Chengbei District, Xining City, Qinghai Province, which has a plateau semi-arid continental climate with the geographical coordinates of 101° 77′ E and 36° 62′ N. The average annual temperature is 7.6 ℃, the elevation is 2 261 m, and the average annual precipitation is 380 mm. The annual average temperature was 7.6 ℃, the altitude was 2 261 m, and the annual average precipitation was 380 mm. The soil for the experiment was taken from the field slope in Chengbei District, Xining City, Qinghai Province, and the soil depth was within 0.3 ~ 1.8 m. Table 1 lists the basic physical properties of the soil samples, which were categorized as loess under the unified soil classification system (USCS). The shrub false indigo bush was selected as the root system research object, which is the native dominant slope protection vegetation in Qinghai Province. It is fast-growing, cold-resistant, barren, drought-resistant, suitable for dry and cold climate in Qinghai Province, with well-developed root system and many lateral roots, and is a good plant for wind and sand control and soil conservation.

Table 1 Basic physical properties of soil

表 1 土体基本参数

Properties	Values	Properties	Values
Specific gravity	2.72	Plasticity Index I_p	19.9
Maximal dry density ρ/g · cm^{-3}	1.66	Optimal moisture content ω/%	16.1
Liquid limit ω_L/%	28.9	Plastic limits ω_p/%	9.0

2.2 *Test program*

2.2.1 Root-soil complex cyclic direct simple shear test

Specimen bottom diameter is 50 mm, height is 20 mm. The dry density of the specimens was 1.6 g/cm^3, the moisture content was 14%, and the root mass ratio was 1.2% (Due to the small size of the specimen, this root content was chosen on the basis of considering the size effect). Because the root system will gradually harden after leaving the soil, in order to reflect the root-soil interaction more realistically, false indigo bush was planted outside the laboratory, and fresh roots excavated on the same day were used in each root-soil complex specimen. First, 0.15 g of fibrous roots less than 0.5 mm in diameter were mixed into the soil and stirred well. The specimen was compacted in two layers, and after the first layer was compacted, three 1.8 mm ~ 2.3 mm diameter root segments were inserted at equal intervals along the shear direction. The flow chart of specimen preparation is shown in Fig 1. After the specimen was consolidated under 100 kPa vertical pressure for 90 min, the corresponding initial shear stress was slowly applied to it and kept for 20 min, at which time the horizontal shear strain of the specimen tended to stabilize. Subsequently, the vertical position of the upper loading plate was kept constant and cyclic shear loads with sinusoidal variations were applied in a stress-controlled manner until the damage criterion was reached. The loading pattern is shown schematically in Fig. 3, which is similar to the cyclic loading scenario in MCCARRON et al[29]. A schematic diagram of the cyclic direct simple shear apparatus (EMDCSS) is shown in Fig. 2. The cyclic direct shear test was performed in accordance with ASTM D6528[56].

In studies of sandy soil liquefaction, many scholars consider that liquefaction of the specimen occurs when the one-way shear strain amplitude reaches 3.75%[57-60]. This damage criterion is not applicable to loess, because the shear strain exceeds 3.75% after a large initial shear

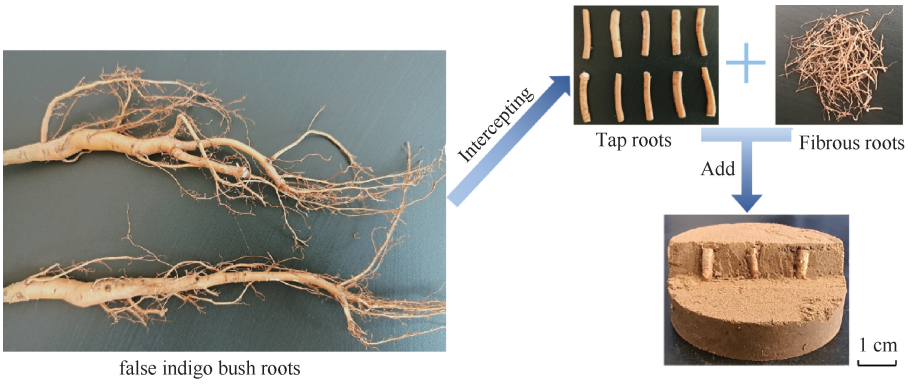

Fig. 1 The flow chart of specimen preparation

图 1 试样制备流程

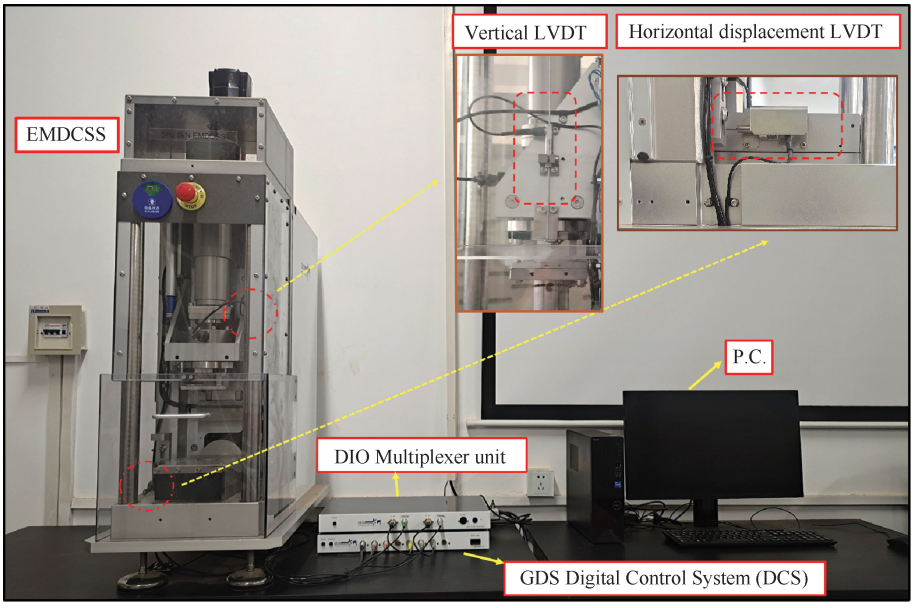

Fig. 2 Dynamic cycle single shear equipment

图 2 动态循环单剪设备

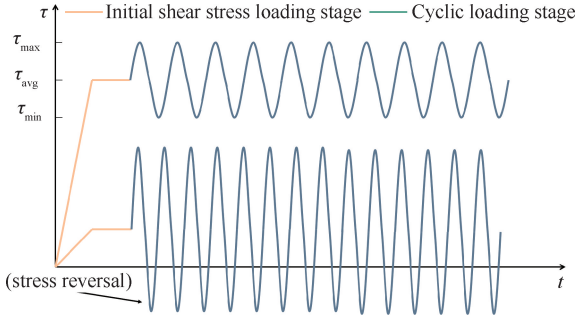

Fig. 3 Loading pattern

图 3 加载方式

stress is applied to the specimen, but the specimen still has certain cyclic shear resistance. Therefore, it is set in this paper that the specimen is considered to be completely damaged when the unidirectional shear strain amplitude exceeds 10%. In the case of larger initial shear stress ratios, the excess pore water pressure after the specimen reaches the damage condition does not necessarily exceed 90% of the initial consolidation pressure, but has remained in a steady state for a period of time in a range smaller than 90% of the consolidation pressure, which is similar to the results of the tests by PARK et al[36]. Therefore, only the residual deformation damage mode is considered, and the cyclic liquefaction damage mode is not considered. The cyclic stress ratio (*CSR*) refers to the ratio of the applied peak cyclic shear stress to the initial vertical consolidation pressure. Initial shear stress ratio (α) means the ratio of initial static shear stress to consolidation pressure. A magnitude 7.5 earthquake generates approximately 15 uniform stress cycles[61], therefore the cyclic resistance of the specimens was quantitatively assessed by using cyclic resistance ratios. The cyclic resistance ratio (*CRR*) refers to the cyclic stress ratio when the specimen reaches the damage criterion after 15 cyclic shear actions. Under the same conditions of consolidation pressure, water content, initial shear stress, and root content, at least four cyclic shear tests with different cyclic stress ratios were conducted to obtain a cyclic resistance curve (*CSR* versus the number of destructive cycles) and consequently, the *CRR* was obtained. Parallel tests were repeated at least twice until the error between the number of destructive cycles was less than 10%. To reflect the effect of initial static shear stress, a correction factor K_α is introduced which is defined as the ratio of *CRR* under any initial shear stress to *CRR* without initial shear stress

$$K_\alpha = \frac{CRR_{\sigma,\,\alpha}}{CRR_{\sigma,\,0}} \tag{1}$$

In group A tests to investigate the effect of initial shear stress on the root-soil composite, the loading frequency was set to 1 Hz, and the initial shear stress ratios were 0.0, 0.1, 0.2, 0.3, and 0.4, respectively. In the group B tests exploring the effect of loading frequency, the initial shear stress ratio was set to 0.15, and the loading frequencies were 0.1 Hz, 0.5 Hz, 1.5 Hz, and 3 Hz, respectively. A total of 75 CDSS tests were conducted, and a detailed description of the test protocol is shown in Table 2.

Table 2 Cyclic direct simple shear test protocol and results

表 2 循环直剪试验方案及结果

Group	No.	Roots	α	Frequency/Hz	*CSR*	*N*	*CRR*	K_α
A	1	No	0.0	1	0.19; 0.2; 0.21; 0.23	169; 86; 32; 22	0.262 1	1.0
	2	No	0.1	1	0.128; 0.135; 0.15; 0.156; 0.16; 0.17; 0.2; 0.3	710; 229; 138; 48; 30; 27; 8; 3	0.179 8	0.69
	3	No	0.2	1	0.1; 0.115; 0.121; 0.126; 0.13; 0.139; 0.144; 0.15	870; 64; 58; 24; 17; 11; 8; 8	0.134 6	0.51
	4	No	0.3	1	0.109; 0.115; 0.126; 0.139; 0.144; 0.154; 0.166; 0.17	139; 39; 29; 12; 15; 7; 5; 4	0.137 8	0.53
	5	No	0.4	1	0.108; 0.115; 0.125; 0.135; 0.156; 0.17; 0.18; 0.19; 0.2; 0.23	125; 63; 35; 23; 18; 9; 7; 6; 5; 3	0.153 2	0.58
	6	Yes	0.0	1	0.2; 0.21; 0.23; 0.243	139; 101; 46; 20	0.214 4	1.0
	7	Yes	0.1	1	0.135; 0.15; 0.16; 0.18	593; 249; 68; 26	0.189 4	0.88
	8	Yes	0.2	1	0.12; 0.125; 0.13; 0.14	169; 38; 28; 14	0.138 6	0.65
	9	Yes	0.3	1	0.109; 0.115; 0.12; 0.126; 0.154	160; 57; 52; 46; 7	0.139 2	0.65
	10	Yes	0.4	1	0.125; 0.135; 0.15; 0.175	114; 73; 19; 10	0.158 4	0.74
B	11	Yes	0.15	0.1	0.11; 0.122; 0.135; 0.155	274; 66; 20; 7	0.140 3	
	12	Yes	0.15	0.5	0.125; 0.133; 0.14; 0.163	159; 80; 29; 12	0.155 7	
	13	Yes	0.15	1.5	0.162; 0.15; 0.135; 0.12	15; 24; 66; 909	0.161 8	
	14	Yes	0.15	3	0.122; 0.137; 0.15; 0.163	169; 63; 36; 24	0.182 3	

Note: $*\alpha$ is initial static shear stress ratio; *N* is the number of destructive cycles

2.2.2 Discrete modeling of monotonic and cyclic direct simple shear tests of rooted soils

The PFC model consists of body, piece, and contact. Contacts hold forces and moments that are applied to the contacting bodies. These forces and moments are calculated based on the force displacement law defined by the contact model. During the simulation, the software (PFC^{3D}) performs a series of operations sequentially within each computational timestep to update the model state: (1) Determine the effective timestep to ensure numerical stability of the model; (2) The position and velocity of each body/piece is updated according to Newton's laws of motion using the current timestep and the forces/moments calculated during the previous cycle; (3) Update model time; (4) Create and delete contacts; (5) Recalculate the forces or moments.

The specimens were first generated within a cylindrical range of 25 mm radius and 20 mm height. When the number of specimen particles is small, the overall mechanical response during loading will be very

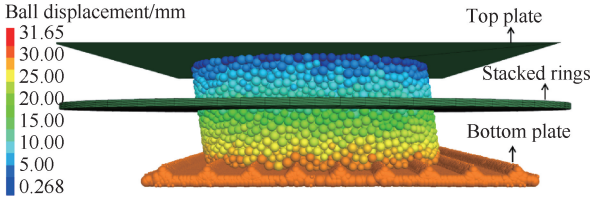

Fig. 4 Schematic diagram of the model

图 4 模型示意

sensitive to the change of individual strong force chain, which causes fluctuation of stress-strain curve. The soil is modeled as an assembly of 14 300 locally interacting spheres under consideration of computational efficiency. The diameters of the particles are uniformly distributed from 0.000 6 m to 0.000 9 m. A jagged clump is created at the bottom of the specimen to simulate the bottom loading plate. 20-layer stacked ring walls were arranged along the specimen height to simulate the lateral boundary. Since the wall does not change its velocity under external forces, the stacked ring walls are given a linearly varying velocity based on the shear direction velocity of the bottom clump as a way to achieve uniform

lateral deformation during shear[62]. The specimen model is shown in Fig. 4. Monotonic shear tests are simulated by assigning constant velocities to the bottom clump; A cyclically varying shear load is transmitted to the specimen by applying a sinusoidally varying external force to the bottom clump. The constant volume shear condition is achieved by fixing the vertical position of the top plate, and the constant pressure (average normal contact stress between the upper wall and the particles) condition is achieved by the servo method. In order to dissipate the kinetic energy of the particles and avoid unrealistic particle vibrations[63], normal and tangential viscous damping (0.1) was applied at each contact, consistent with the values used by ZHANG et al[49]. The maximum dimensionless inertia number during the simulation is $7.2e^{-4}$, less than $1e^{-3}$, which is enough to prohibit potential inertial effect, meaning that the granular assembly behaviors are quasi-static.

In the previous modeling process of root-soil composites, special elements (such as: deformable cylinders, cable, beam, truss) were introduced to simulate the root system[38,64-65]. In this paper, a string of inter-bonded particles is used to simulate the root system, with coarse and fibrous roots arranged in the same manner as described in section 2.2.1. To avoid the effect of root incorporation on the porosity of the specimen, the loess particles at the location of the root particles were deleted. A customized contact model more suitable for cohesive granular material[66-67] was used between loess particles, and the corresponding force-displacement law is shown schematically in Fig. 5. The established contact model is based on the linear parallel-bond contact model and refined the force displacement law between particles after the bonding strength reaches the critical bonding strength. This contact model can effectively capture the softening behavior of cohesive material during cyclic shear and has high computational efficiency. Parallel-bond contact model was used both between root particles and between root-soil particles. Thus, the model allows simulating the root tensile loading until broken, the root bending loading, the root compression loading, the root-soil adhesive links until bonding breakage, the root slippage associated with a frictional resistance at the root-soil interface.

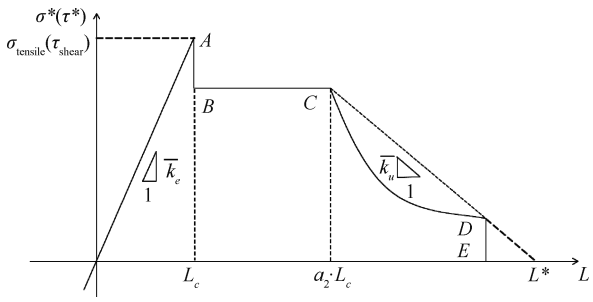

Fig. 5 Schematic diagram of the force-displacement law

图 5 力-位移定律示意

3 Results and discussion

3.1 *Cyclic direct simple shear test results*

3.1.1 Cyclic resistance response of specimens under different initial shear stress

In the absence of the initial shear stress, the shear strain will oscillate with the x-axis as the symmetry axis at the beginning of loading, and no plastic strain will be generated. If the specimen is sudden runaway damage pattern, after a certain number of cycles, the shear strain will accumulate rapidly in one direction and the effective stress suddenly reaches zero, thus producing damage. If the specimen is cyclic mobility damage pattern, the plastic shear strain accumulation gradually occurs at the later stages of loading and shear strain slowly reaches the damage criterion. On the contrary, in the presence of initial shear stress, the specimen will accumulate plastic strain in the direction of the initial shear stress applied from the beginning. The results of all cyclic direct simple shear tests are summarized in Table 2.

Fig. 6 shows the cyclic resistance curves of loess and the root-soil composite under different initial shear stress ratios (α) with the consolidation pressure and loading frequency held at 100 kPa and 1 Hz, respectively. It can be seen from the figure that the cyclic resistance of the root-soil composite shows an evolutionary pattern similar to that of the loess with the increase of the initial shear stress. As α increased from 0.0 to 0.2, the cyclic resistance curves of the loess and root-soil composites gradually shifted downward, with *CRR* decreasing by 49% and 35%, respectively. When α increased to 0.3, the cyclic resistance increased slightly by 2.4% and 0.4%. When α was further increased to 0.4, there was a significant recovery in cyclic resistance to 58% and 74%

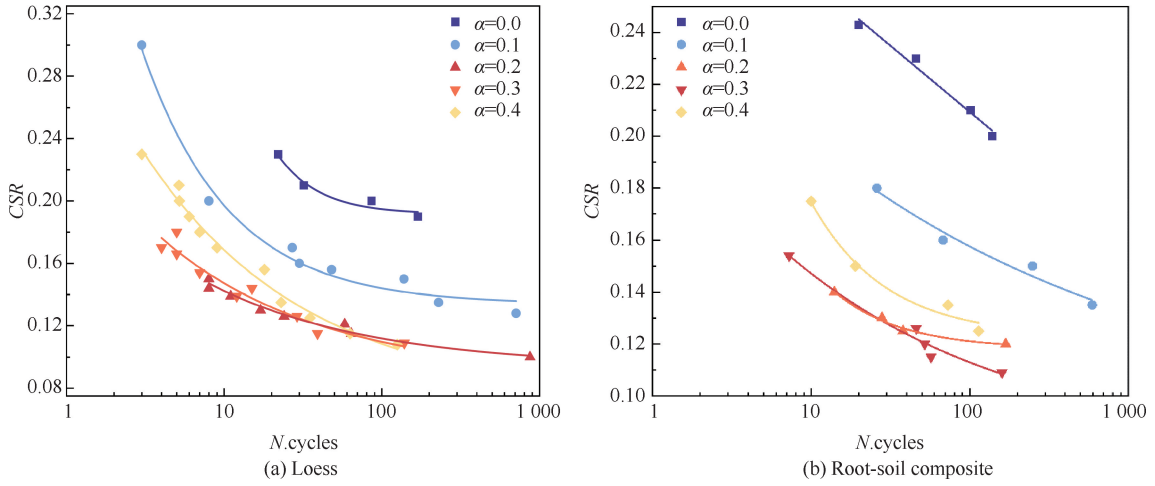

Fig. 6 Cyclic resistance curves under different initial shear stress ratios

图 6 不同初始剪应力比下的循环阻力曲线

of the strength without initial shear stress, respectively. However, the cyclic resistance of specimen without initial shear stress is always higher than the resistance with initial shear stress. The presence of initial shear stress always acts as an unfavorable factor for the cyclic resistance of the specimens. The decrease in the cyclic resistance of specimen with increasing α is due to the fact that the loading of horizontal stresses under the rotational condition of the principal stresses induces a breakage of the loess inter-particle bond and root-soil bond. At the same time, the larger the value of α, the less likely the specimen is to undergo a stress reversal situation, and thus the more likely it is to produce a rapid accumulation of plastic strain in one direction, leading to a decrease in cyclic resistance. The reason for the rebound of the cyclic resistance of specimen with the further increase of α is due to the fact that, in response to the greater horizontal shear stress action, the interparticle structure of the specimen is rearranged and the interlocking effect is enhanced, which further forms a stable substrata structure and establishes a stronger and more tight horizontal-oriented contact and force chain.

The effect of root system on the cyclic resistance ratio (*CRR*) under different initial shear stresses is shown in Fig. 7. In the presences of root system, *CRR* increases regardless of the value of α. As the value of α increased, the incremental strength of cyclic resistance induced by the root system showed a first decreasing and then increasing pattern. As the initial shear stress increases, the initial shear strain of the specimen also becomes larger, which leads to a smaller range of mutual frictional sliding between the roots and the soil during the reciprocal cycle, reducing the consumption of the input shear action energy and thus weakening the reinforcing effect. In this process, the change of specimen fabric structure also has a potential influence on the performance of root system reinforcement. When the α value increased to 0.4, the initial shear strain of the specimen reached about 5%. The initial inclination angle of the root system was too large, and the specimen fabric structure changed significantly, thus affecting the development pattern of the reinforcement action.

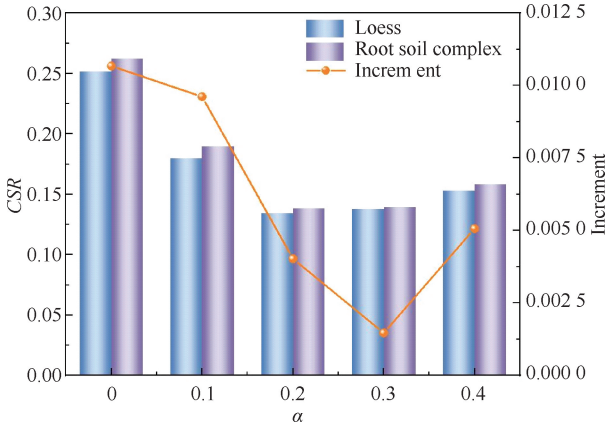

Fig. 7 Comparison of *CRR* values of loess and root-soil composite under different initial shear stress ratios

图 7 不同初始剪应力比下黄土和根土复合体的 *CRR* 对比

3.1.2 Cyclic resistance response of specimens under different frequency

In order to investigate the effect of cyclic loading frequency on shear behavior, CDSS tests were conducted

on root-soil composites at different frequencies. The cyclic resistance curves of the root-soil composite at 0.1 ~ 3 Hz frequencies are shown in Fig. 8. From the figure, it can be seen that the cyclic resistance strength of the root-soil composite is affected by the frequency with CRR as 0.140, 0.156, 0.162, 0.182 at 0.1, 0.5, 1.5, 3 Hz respectively. As the loading frequency increases, the position of the cyclic resistance curve of the root-soil composite shifts upward and the cyclic resistance continues to increase. NONG et al[68-69] also came to a similar conclusion that an increase in cyclic shear frequency decreases the rate of accumulation of volumetric strain in sandy soils and increases the shear modulus ratio (the ratio of the shear modulus after a certain number of cycles to the initial shear modulus), which in turn increases the liquefaction resistance. Actual seismic loads are a mixture of various frequencies in a certain interval, so the dynamic mechanical properties of root-soil complexes derived by the laboratory at lower frequencies may underestimate the stability of root-containing slopes. Under high-frequency loading, the specimens do not have enough time to deform during the rapid loading process and the rate of plastic accumulation is slow. However, under low-frequency loading, the specimens produce sufficient deformation and the residual strain after each cyclic action is larger, so the cyclic resistance strength of the root-soil composite under low-frequency loading is lower.

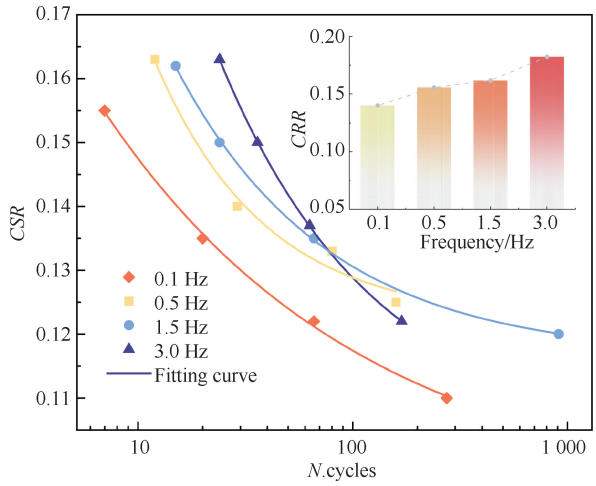

Fig. 8 Cyclic resistance curves of root-soil composite under different loading frequencies

图 8 不同加载频率下根土复合体的循环阻力曲线

3.1.3 Reinforcement mechanism of root system

Scanning electron microscopy results for roots are presented in Fig. 9 at magnifications of 50, 100, and 1 000, respectively. It can be seen that the surface of the root system is uneven, and the loess particles become embedded in the grooves of the root system, and the two bite and nest each other. Roots secrete chemicals substances (sugars, organic acids, etc.) that act as cementing agents during the growth process, increasing the strength of the bonds between loess particles. Due to the difference in deformation modulus between the root system and the loess matrix, the inclination angle of the root segment is not the same as that of the specimen as a whole ($\alpha \neq \beta$, which is shown in Fig. 10) under any horizontal shear strain, resulting in frictional sliding between the two phases of the root-soil, thus dissipating some of the incoming shear energy from the base. The uniformly distributed fibrous roots and soil particles in the specimen are intertwined with each other, which improves the integrity of the specimen, and the three-dimentional network structure formed by the lap between the fibrous roots effectively limits the displacement of the soil particles. As long as the fibrous root does not produce complete sliding with the surrounding soil unit, it will pull the soil body at both sides of the microcracks and

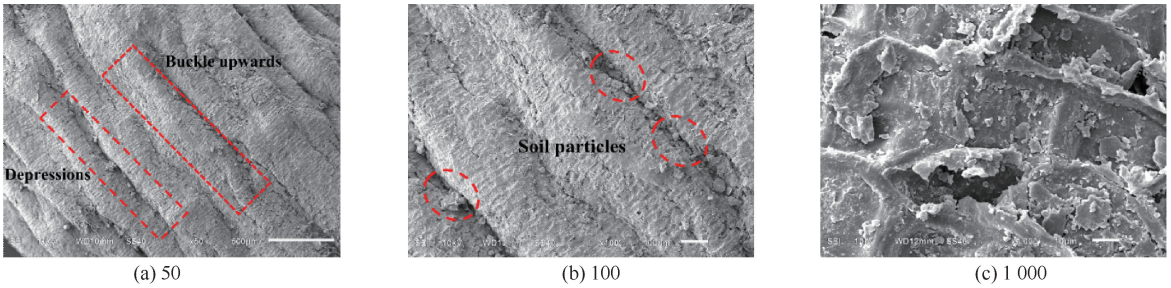

(a) 50 (b) 100 (c) 1 000

Fig. 9 Scanning electron microscopy results at magnifications of 50, 100 and 1 000

图 9 放大 50、100 和 1 000 倍的扫描电镜结果

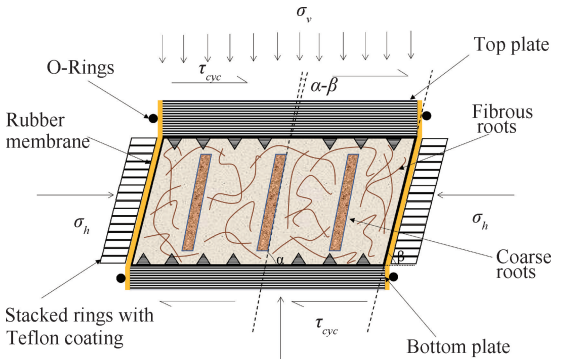

Fig. 10 Schematic diagram of root reinforcement mechanism

图 10 根系强化机理示意

inhibit the further development of the crack, that is, to bridge microcracks[70]. Part of the shear stress in the specimen is transferred to the root system, which is stored as tensile strain energy, further consuming the external input shear energy, thus improving the cyclic resistance of the loess.

3.2 *Shear simulation results of root-soil complex*

3.2.1 Cyclic direct simple shear simulation results for the non-rooted soil

Cyclic shear simulations at constant volume without initial shear stress for non-rooted soil samples were first performed at cyclic stress ratios of 0.22, 0.23, and 0.243, respectively, with an initial vertical consolidation pressure of 100 kPa. The objective is to evaluate the relevancy of the new customized contact model for modeling loess and to provide reference simulation results for the comparison between the cyclic resistance of non-rooted and rooted soils. The simulation-derived shear stress-shear strain curves are shown in Fig. 11 (a-c). After the specimen experiences the stress-strain state shown in the figure, the shear strain increases rapidly and reaches the damage criterion, and this section of the curve is not plotted in the figure. Under the use of the modeling approach and contact model proposed in this paper, the simulation results can capture the response behavior of the loess specimens in terms of stiffness degradation and shear strain accumulation under cyclic shear loading. The simulation results also show that an increase in the applied cyclic shear stress ratio induces a decrease in the number of cyclic loading required for specimen destruction, as would be expected. From

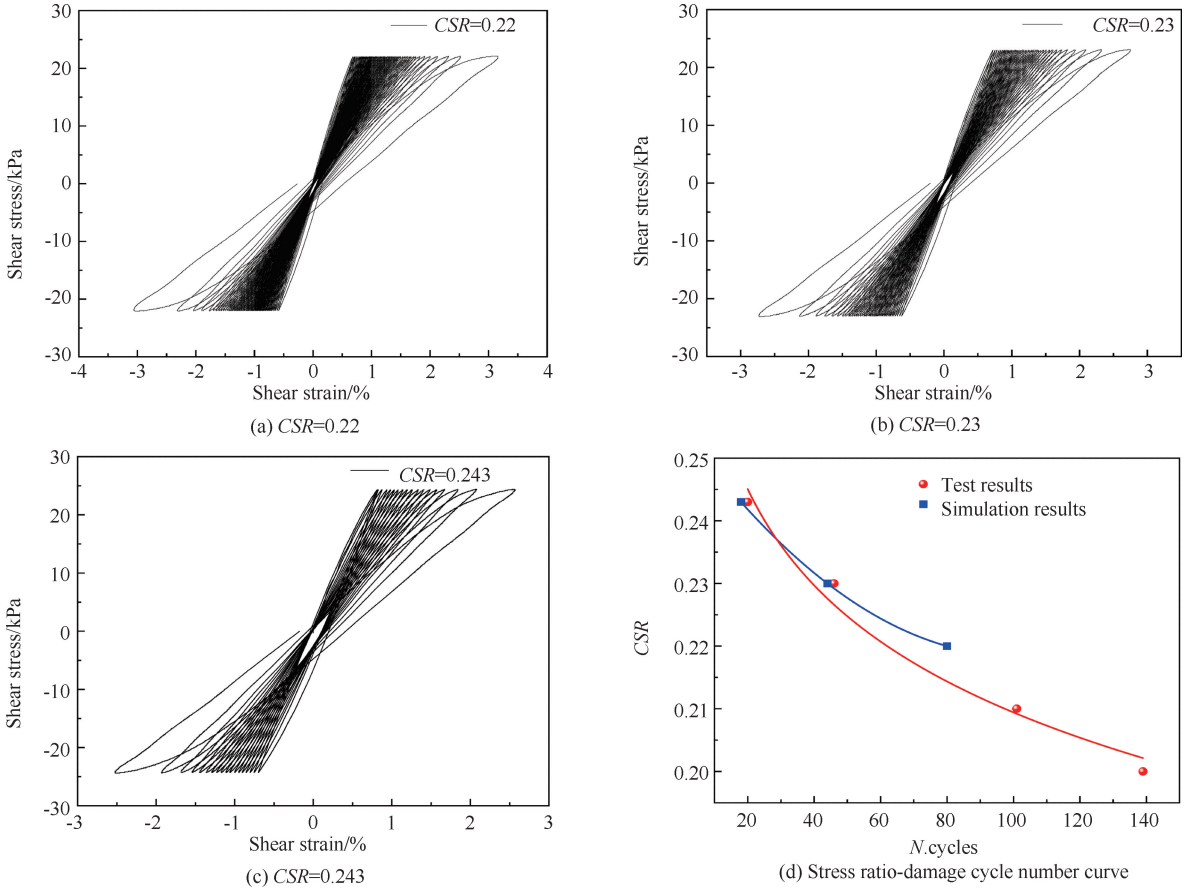

Fig. 11 Simulation results of cyclic direct simple shear

图 11 循环直剪模拟结果

Fig. 11(d), it can be seen that the cyclic resistance curves derived from simulation and test are in high agreement, which proves the reasonableness of the contact model and model parameters. The values of the selected meso-parameters are shown in Table 3. The stress-strain curve shows butterfly-shaped hysteresis loops when the specimen is near the damage state, but the simulation results do not have this phenomenon. The reasons may be the forced linear variation of wall velocity assignment, the difference between spherical soil model particles and the actual soil particles shape, the limitation of the number of particles, and other factors.

Table 3 Meso parameters used for new contact model

表 3 用于新接触模型的细观参数

Property	Symbol	Values	
		Monotonic shear	Cyclic direct simple shear
Effective modulus	emod	5.0×10^7	1.0×10^7
Stiffness ratio	kratio	1.5	1.5
Friction angle/(°)	fa	30	30
Friction-ball-ball	fric	0.1	0.1
Friction-ball-sidewall	fric	0.0	0.0
Friction-ball-upwall	fric	0.5	0.5
Normal bonding strength	ten	1.2×10^4	1.2×10^4
Tangential cohesion strength	coh	1.2×10^4	1.2×10^4
Normal critical damping	β_n	0.13	0.1
Tangential critical damping	β_s	0.13	0.1
$AB/\sigma_{tensile}$	α_1	0.7	0.8
BC/L_c	α_2	3.0	10.0
$\overline{k_u}/\overline{k_e}$	δ_1	9.0	4.0
$CD/\sigma_{tensile}$	δ_2	0.2	0.2
Particle density	ρ	2 700	2 700
Frequency/Hz	f	—	1
Shear stress amplitude/kPa	τ_{cyc}	—	22; 23; 24.3

Note: "—" implies no such item.

3.2.2 Cyclic direct simple shear simulation results for the root-soil composite

During the CDSS simulation, not all roots develop tensile stresses, and some of them show compressive deformation, as well as alternating tensile and compressive changes as the shear proceeds. FAN et al[71] came to the same phenomenon through monitoring root forces developed in a plant root system subjected to in-situ large shear. However, most of the predictive models for the shear strength of rooted soils do not consider the roots that develop compressive forces, and focus only on the mechanical reinforcement of the soil by the roots in tensile mode.

The elastic modulus of the roots is an important characteristic that influences the shear strength of soils[72-73], but compared to the tensile strength of the root system, it has rarely been discussed, and its effect on the cyclic resistance of root-soil composite is unknown. The contact model between root particles was chosen as the linear parallel-bond contact model, and the change of contact stiffness parameter (pb_deform) can qualitatively reflect the change of root elastic modulus, so different pb_deform parameters were chosen for the cyclic simple shear simulation test. The initial effective consolidation stress was set to 100 kPa, the cyclic shear stress ratio was set to 0.243, and the loading frequency was 1 Hz during simulation process. Fig. 12 shows the variation of shear strain with loading time and shear stress with shear strain for different contact stiffness parameters. Rooted soil specimens were completely destroyed after 42, 40, 33, 29, 16 cyclic actions at pb_deform of 10×10^6, 5×10^6, 2.5×10^6, 1.3×10^6, and 0.1×10^6, respectively. Therefore, as the elastic modulus of the root system increases, the number of loadings required for the root-soil composite specimen to reach the damage condition is increasing, i.e., the cyclic resistance is increasing. MAO et al[38] reached similar conclusions through finite element direct shear simulations, that higher root elastic modulus would be more effective in increasing the shear strength of the soil at all different initial root orientations. The relationship between root elastic modulus and diameter can be described by the negative power-law function[20,74]. However, different vegetation has different function parameters, so when selecting species for slope protection, it is better to use vegetation with higher root elastic modulus. The effect of bending resistance of roots on shear resistance is relatively small for cohesive and frictional granular soils[50], thus this paper does not analyze the effect of bending resistance on rooted loess.

The root-soil bond strength (maximum tangential shear stresses mobilized at the root-soil interface) is a key input parameter in root-added soil shear strength prediction models (e.g., Simple Force Balance Model WWM, Fiber Bundle Model FBM), but it is not directly and accurately obtainable[74]. Therefore, the influence of root-soil interfacial bond strength on root reinforcement

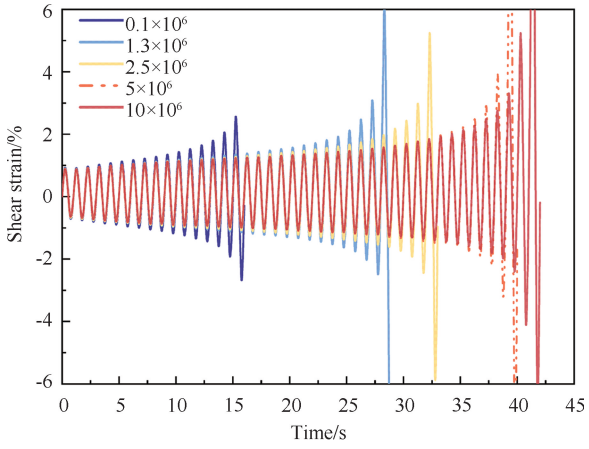

(a) Shear strain versus loading time curves

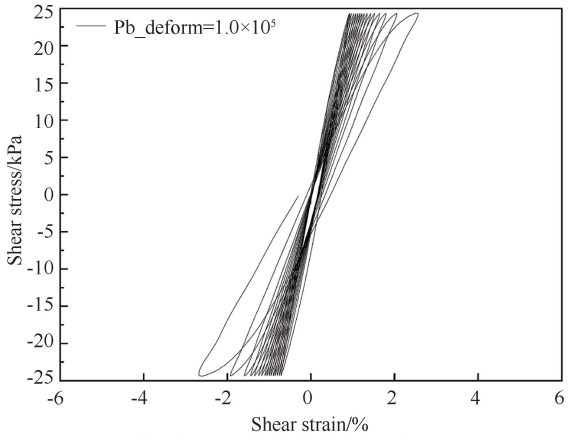

(b) Shear stress versus shear strain curves (Pb_deform=1.0×10⁵)

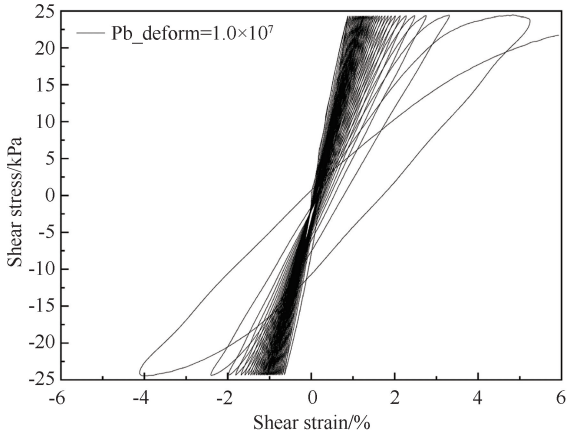

(c) Shear stress versus shear strain curves (Pb_deform=1.0×10⁷)

Fig. 12 The simulation results at different Pb_deform parameters

图 12 不同的 Pb_deform 参数模拟结果

effect under cyclic shear loading needs to be investigated. A linear parallel-bond contact model was chosen to model the contact between roots and loess particles, and the decrease in bond strength between roots and soil was simulated by continuously decreasing the parameters Pb_ten, Pb_coh, fric. The variation of root-soil composite shear strain with loading time and shear stress with shear strain for different bonding parameters is shown in Fig. 13. The number of damage cycles for the root-soil composite specimens were 42, 39, 26, 23, 20 at bond

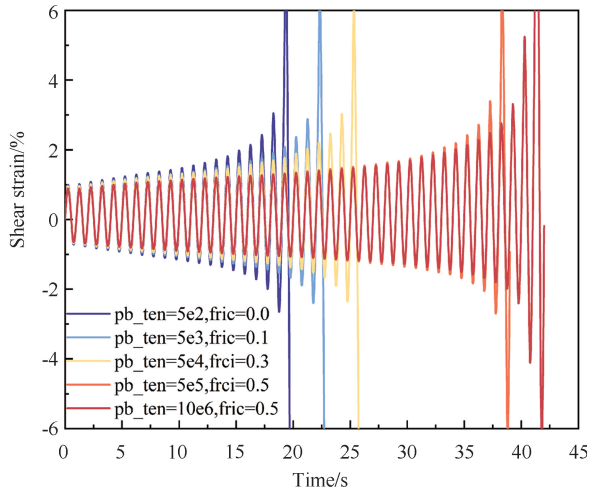

(a) Shear strain versus loading time curves

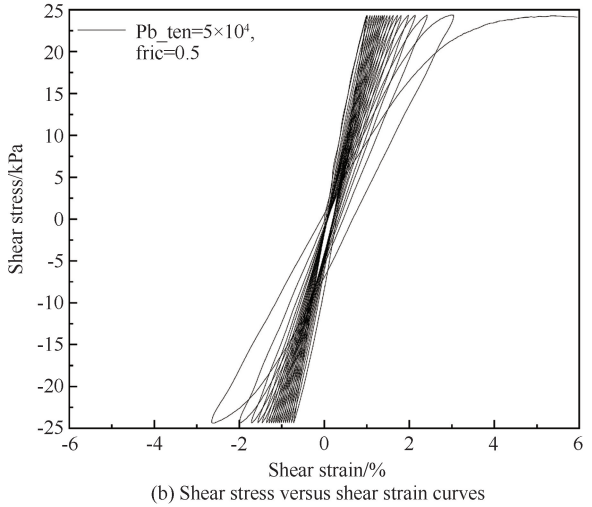

(b) Shear stress versus shear strain curves (Pb_ten=5×10⁴)

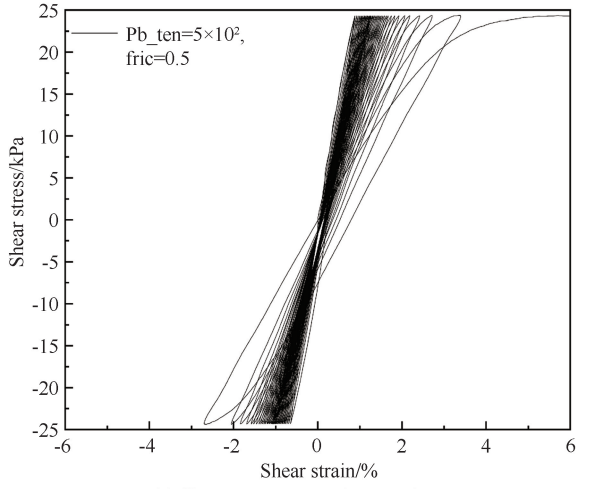

(c) Shear stress versus shear strain curves (Pb_ten=5×10²)

Fig. 13 The simulation results at different Pb_ten parameters

图 13 不同 Pb_ten 参数下的模拟结果

strengths of 10×10^6, 5×10^5, 5×10^4, 5×10^3, 5×10^2 Pa, respectively. The results showed that the cyclic resistance of the root-soil composite continued to decrease as the strength of the root-soil interfacial bond decreased. At higher root-soil interfacial bond strength, the root system is less prone to sliding and the tensile strength can be fully mobilized, thus more of root's potential for reinforcement could be realized. When there is a breakdown of the partial bonding between roots and loess particles and they slide against each other, the higher friction strength dissipates more shear energy, thus increasing the cyclic resistance of the root-soil composite. When the root system possess numerous, spreading, highly-branched fibrous roots, the bond strength between the root-soil is significantly increased compared to non-branching, smooth roots. Therefore, vegetation with a high degree of root epidermal roughness and well-developed fibrous roots should be prioritized in the selection of vegetation for slope protection. Under storm events, transpiration from vegetation is difficult to resist the saturating effects of rainfall[75], resulting in a significant reduction in the bonding strength between root-soil. Therefore, the contribution of vegetation to the slope stability factor of safety under heavy rainfall conditions is less than that under non-rainfall conditions, and the slope protection effect of vegetation should be assessed conservatively.

The orientation of the root system relative to the shear plane affects the stress developed in roots and the shear strength of the rooted soil[76-77], so this section explores the effect of root orientation on the cyclic resistance of the specimen. The angles between the root direction and the horizontal plane were arranged as 0°, 30°, 60°, and 90°, respectively, and the cyclic simple shear simulation was performed by applying a cyclic shear stress ratio of 0.243 at a frequency of 1 Hz. The simulation results are shown in Fig 14. The number of damage cycles for the root-soil composite specimens was 42, 39, 26, 23 under 0°, 30°, 60°, and 90° root orientation, respectively. The maximum and minimum cyclic resistance is obtained when the angle between the root system and the horizontal plane is 90° and 0°. JEWELL et al[78] came to a similar conclusion that little or no increase in shear strength is obtained when the root system is parallel to the shear plane during the direct shear test. Fig. 14(b) shows the variation of tensile stress between all root particles with loading time. The tensile stresses mobilized by the horizontal root system are relatively small, resulting in the lowest contribution of the root system to the cyclic resistance strength of the soil. However, the tensile stresses mobilized by the vertically arranged root system are also small, due to the initial vertical consolidation stresses that result in large compressive stresses in the root system at the outset. The direction of the specimen principal stresses varied in the range of 0° ~ 30° over the vast majority of the cyclic loading period. The vertically arranged root system is approximately perpendicular to the direction of the principal stresses and therefore has the greatest cyclic resistance.

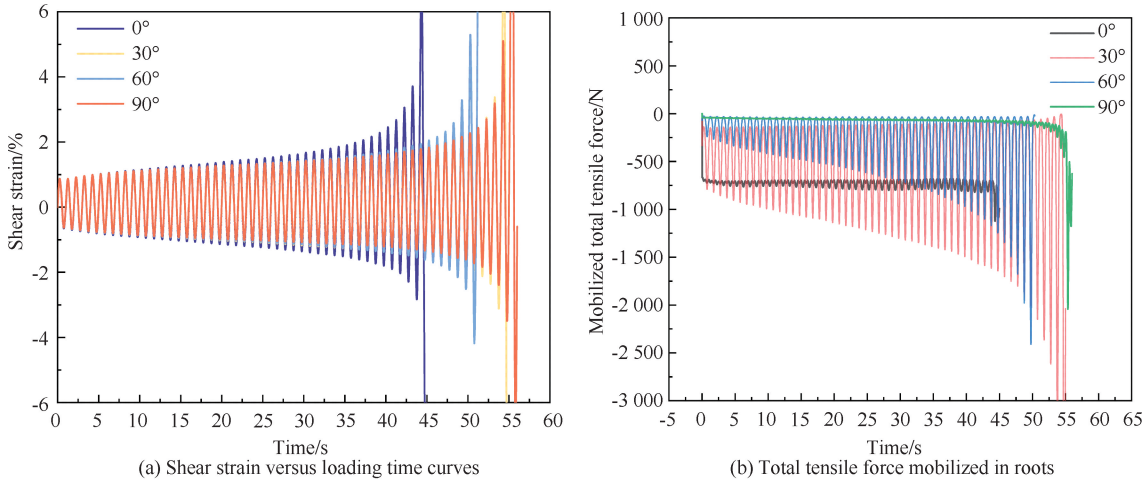

(a) Shear strain versus loading time curves　(b) Total tensile force mobilized in roots

Fig. 14　The simulation results at different root orientation

图 14　不同根系方向模拟结果

4 Conclusion

In this paper, a series of stress-controlled constant volume cyclic direct simple shear tests were conducted to analyze the reinforcing effect of roots on the cyclic resistance of loess, as well as the effects of initial static shear stress and loading frequency on the cyclic resistance of root-soil composites. A numerical model based on the Discrete Element Method was developed and used in this study to analyze the effects of root geometry, mechanical properties, and root-soil interactions on cyclic resistance.

(1) Under the cyclic shear damage criterion defined in this paper, the presence of the root system improves the cyclic resistance strength of the loess. The experimental results provide a justification for the slope protection effect of the root system under dynamic action (earthquakes or waves). When the consolidation pressure and loading frequency are kept constant, with the increase of the initial shear stress ratio, the cyclic resistance of the loess and root-soil composite shows a law of first decreasing and then rebounding; when the consolidation pressure and initial shear stress ratio are kept constant, with the increase of the loading frequency, the cyclic resistance of the root-soil composite shows a law of continuously increasing;

(2) The shear simulation methodology adopted in this paper and the contact model developed for cohesive granular material can effectively reproduce the mechanical response of root-soil composites under cyclic shear conditions.

(3) Increases in both root elastic modulus and root-soil interfacial bond strength can effectively enhance the cyclic resistance of root-soil composites. The maximum cyclic resistance strength is obtained when the initial arrangement of the root system is oriented at an angle of 90° to the horizontal plane; the lowest cyclic resistance strength is obtained when the root system is oriented horizontally. Therefore, when selecting vegetation for slope protection, plants with higher root modulus of elasticity, higher root epidermal roughness and well-developed fibrous roots should be selected among the locally dominant growing species, and vegetation with plateroot root systems should be avoided.

参考文献:

[1] SCHENK H J, JACKSON R B. The global biogeography of roots [J]. Ecological Monographs, 2002, 72(3): 311.

[2] FAN C C, SU C F. Role of roots in the shear strength of root-reinforced soils with high moisture content [J]. Ecological Engineering, 2008, 33(2): 157-166.

[3] SCHMALTZ E M, STEGER S, GLADE T. The influence of forest cover on landslide occurrence explored with spatio-temporal information[J]. Geomorphology, 2017, 290: 250-264.

[4] WALDRON L J. The shear resistance of root-permeated homogeneous and stratified soil [J]. Soil Science Society of America Journal, 1977, 41(5): 843-849.

[5] MASI E B, SEGONI S, TOFANI V. Root reinforcement in slope stability models: a review[J]. Geosciences, 2021, 11(5): 212.

[6] POLLEN N. Temporal and spatial variability in root reinforcement of streambanks: Accounting for soil shear strength and moisture [J]. Catena, 2007, 69(3): 197-205.

[7] GREENWAY D R. Vegetation and Slope Stability[M]. New York: Wiley Press, 1987.

[8] BRUAND A, COUSIN I, NICOULLAUD B, et al. Backscattered electron scanning images of soil porosity for analyzing soil compaction around roots[J]. Soil Science Society of America Journal, 1996, 60(3): 895-901.

[9] GUIDI G, POGGIO G, PETRUZZELLI G. The porosity of soil aggregates from bulk soil and from soil adhering to roots[J]. Plant and Soil, 1985, 87(2): 311-314.

[10] TISDALL J M, COCKROFT B, UREN N C. The stability of soil aggregates as affected by organic materials, microbial activity and physical disruption[J]. Soil Research, 1978, 16(1): 9.

[11] YOUNG I M. Biophysical interactions at the root-soil interface: A review[J]. The Journal of Agricultural Science, 1998, 130(1): 1-7.

[12] MUZYLO A, LLORENS P, VALENTE F, et al. A review of rainfall interception modelling [J]. Journal of Hydrology, 2009, 370(1): 191-206.

[13] CHEN Z F, LI H, JIANG N S. Freeze-thaw time and moisture content affect shear strength of loess reinforced with Sophora japonica roots[J]. Bulletin of Soil and Water Conservation, 2023, 43(2): 43-49.

[14] WU T H, MCKINNELL W P, SWANSTON D N. Strength of tree roots and landslides on prince of Wales Island, Alaska [J]. Canadian Geotechnical Journal, 1979, 16(1): 19-33.

[15] DE BRITO GALVÃO T C, PEREIRA A R, PARIZZI M G, et al. Bioengineering techniques associated with soil nailing applied to slope stabilization and erosion control[J]. Natural Hazards Review, 2010, 11(2): 43-48.

[16] FAN C C. A displacement-based model for estimating the shear resistance of root-permeated soils[J]. Plant and Soil, 2012, 355(1/2): 103-119.

[17] ABE K, ZIEMER R R. Effect of tree roots on a shear zone: Modeling reinforced shear stress [J]. Canadian Journal of Forest

Research, 1991, 21(7): 1012-1019.

[18] SCHWARZ M, LEHMANN P, OR D. Quantifying lateral root reinforcement in steep slopes-from a bundle of roots to tree stands[J]. Earth Surface Processes and Landforms, 2010, 35(3): 354-367.

[19] POLLEN N. Temporal and spatial variability in root reinforcement of streambanks: Accounting for soil shear strength and moisture[J]. Catena, 2007, 69(3): 197-205.

[20] JI J N, MAO Z, QU W B, et al. Energy-based fibre bundle model algorithms to predict soil reinforcement by roots[J]. Plant and Soil, 2020, 446(1/2): 307-329.

[21] LIANG T, KNAPPETT J A. Centrifuge modelling of the influence of slope height on the seismic performance of rooted slopes [J]. Géotechnique, 2017, 67(10): 855-869.

[22] KARIMZADEH A A, LEUNG A K, HOSSEINPOUR S, et al. Monotonic and cyclic behaviour of root-reinforced sand[J]. Canadian Geotechnical Journal, 2021, 58(12): 1915-1927.

[23] BERNHARDT M L, BISCONTIN G, O'SULLIVAN C. 3D discrete element method simulations of a laminar-type simple shear apparatus [C]//ASCE. Geo-Congress 2014: For Sustainability 2014. San Diego, CA(US): Geotechnical Special Publication, 2014: 614-623.

[24] AL TARHOUNI M A, HAWLADER B. Monotonic and cyclic behaviour of sand in direct simple shear test conditions considering low stresses[J]. Soil Dynamics and Earthquake Engineering, 2021, 150: 106931.

[25] LASHKA R I, FALSAFIZAD E H, RAHMAN M. Influence of linear coupling between volumetric and shear strains on instability and post-peak softening of sand in direct simple shear tests[J]. Acta Geotechnica, 2021, 16(11): 1-22.

[26] LBIBB S, MANZARI M T. Stress-strain behavior of Ottawa sand in cyclic direct simple shear and modeling of cyclic strength using Artificial Neural Networks [J]. Soil Dynamics and Earthquake Engineering, 2023, 164: 107585.

[27] LIU F C, CHEN L, WANG H D. Evaluation of dynamic shear modulus and damping ratio of rubber-sand mixture based on cyclic simple shear tests[J]. Rock and Soil Mechanics, 2016, 37(7): 1903-1913.

[28] WANG Q, ZHANG Z, SHAO S J, et al. Experimental study on seismic compression of Chinese loess under cyclic direct simple shear testing[J]. Advances in Civil Engineering, 2022, 2022(9): 5689912.

[29] MCCARRON W, LAWRENCE J, WERNER R, et al. Cyclic direct simple shear testing of a Beaufort Sea clay[J]. Canadian Geotechnical Journal, 1995, 32(4): 584-600.

[30] ELGHORAIBY M A, PARK H, MANZARI M T. Stress-strain behavior and liquefaction strength characteristics of Ottawa F65 sand [J]. Soil Dynamics and Earthquake Engineering, 2020, 138: 106292.

[31] YE B, LU J F, YE G L. Pre-shear effect on liquefaction resistance of a Fujian sand[J]. Soil Dynamics and Earthquake Engineering, 2015, 77: 15-23.

[32] CHIARO G, KOSEKI J, SATO T. Effects of initial static shear on liquefaction and large deformation properties of loose saturated Toyoura sand in undrained cyclic torsional shear tests [J]. Soils and Foundations, 2012, 52(3): 498-510.

[33] NEMAT-NASSER S, TOBITA Y. Influence of fabric on liquefaction and densification potential of cohesionless sand[J]. Mechanics of Materials, 1982, 1(1): 43-62.

[34] YANG J, SZE H Y. Cyclic behaviour and resistance of saturated sand under non-symmetrical loading conditions[J]. Géotechnique, 2011, 61(1): 59-73.

[35] VAID Y P, CHERN J C. Effect of static shear on resistance to liquefaction[J]. Soils and Foundations, 1983, 23(1): 47-60.

[36] PARK S S, NONG Z Z, LEE D E. Effect of vertical effective and initial static shear stresses on the liquefaction resistance of sands in cyclic direct simple shear tests[J]. Soils and Foundations, 2020, 60(6): 1588-1607.

[37] MICKOVSKI S B, STOKES A, VAN BEEK R, et al. Simulation of direct shear tests on rooted and non-rooted soil using finite element analysis[J]. Ecological Engineering, 2011, 37(10): 1523-1532.

[38] MAO Z, YANG M, BOURRIER F, et al. Evaluation of root reinforcement models using numerical modelling approaches [J]. Plant and Soil, 2014, 381(1/2): 249-270.

[39] CUNDALL P A, STRACK O D L. A discrete numerical model for granular assemblies[J]. Géotechnique, 1979, 29(1): 47-65.

[40] JIANG M J, YAN H B, ZHU H H, et al. Modeling shear behavior and strain localization in cemented sands by two-dimensional distinct element method analyses[J]. Computers and Geotechnics, 2011, 38(1): 14-29.

[41] XU D S, TANG J Y, ZOU Y, et al. Macro and micro investigation of gravel content on simple shear behavior of sand-gravel mixture[J]. Construction and Building Materials, 2019, 221: 730-744.

[42] DABEET A. Discrete Element Modeling of Direct Simple Shear Response of Granular Soils And Model Validation Using Laboratory Tests[D]. Vancouver: University of British Columbia, 2014.

[43] ASADZADEH M, SOROUSH A. Fundamental investigation of constant stress simple shear test using DEM[J]. Powder Technology, 2016, 292: 129-139.

[44] AI J, LANGSTON P A, YU H S. Discrete element modelling of material non-coaxiality in simple shear flows [J]. International Journal for Numerical and Analytical Methods in Geomechanics, 2014, 38(6): 615-635.

[45] ASADZADEH M, SOROUSH A. Macro - and micromechanical evaluation of cyclic simple shear test by discrete element method[J]. Particuology, 2017, 31: 129-139.

[46] BERNHARDT M L, BISCONTIN G, O'SULLIVAN C. Experimental validation study of 3D direct simple shear DEM simulations[J]. Soils and Foundations, 2016, 56(3): 336-347.

[48] ASADZADEH M, SOROUSH A. Evaluation of stress and strain non-uniformity during cyclic simple shear test using DEM: Effect of the horizontal platen asperities[J]. Granular Matter, 2018, 20(3): 43.

[49] ZHANG L, EVANS T M. Investigation of initial static shear stress effects on liquefaction resistance using discrete element method simulations[J]. International Journal of Geomechanics, 2020, 20

(7): 04020087.

[50] BOURRIER F, KNEIB F, CHAREYRE B, et al. Discrete modeling of granular soils reinforcement by plant roots[J]. Ecological Engineering, 2013, 61: 646-657.

[51] DABEET A, WIJEWICKREME D, BYRNE P. Simulation of cyclic direct simple shear loading response of soils using discrete element modeling[C]//IAEE. Proceedings of the 15th World Conference on Earthquakes Engineering. Lisbon, Portugal: Sociedade Portuguesa de Engenharia Sismica, 2012: 10780316.

[52] CIANTIA M O, PREVITALI M, CAKIR T. Experimental and DEM study of monotonic and cyclic simple shear testing of an angular sand [C]//RAHMAN M M. Proceedings of the 20th International Conference on Soil Mechanics and Geotechnical Engineering. Sydney: Australian Geomechanics Society, 2021: 141802.

[53] O' SULLIVAN C, CUI L, STUART C O' N E I L L. Discrete element analysis of the response of granular materials during cyclic loading[J]. Soils and Foundations, 2008, 48(4): 511-530.

[54] MA Y, HUANG H. DEM analysis of failure mechanisms in the intact Brazilian test [J]. International Journal of Rock Mechanics and Mining Sciences, 2018, 102: 109-119.

[55] JIANG M, LIU J, SHEN Z F, et al. Exploring the critical state properties and major principal stress rotation of sand in direct shear test using the distinct element method[J]. Granular Matter, 2018, 20: 1-18.

[56] TANG C S, SHI B, ZHAO L Z. Interfacial shear strength of fiber reinforced soil[J]. Geotextiles and Geomembranes, 2010, 28(1): 54-62.

[57] VAID Y P, SIVATHAYALAN S. Static and cyclic liquefaction potential of Fraser Delta sand in simple shear and triaxial tests[J]. Canadian Geotechnical Journal, 1996, 33(2): 281-289.

[58] KIM S J. Behavior of Sand in Cyclic Simple Shear Test[D]. Busan: Pusan University, 2009.

[59] ISHIHARA K. Liquefaction and flow failure during earthquakes[J]. Geotechnique, 1993, 43(3): 351-451.

[60] SIVATHAYALAN S, HA D. Effect of static shear stress on the cyclic resistance of sands in simple shear loading[J]. Canadian Geotechnical Journal, 2011, 48(10): 1471-1484.

[61] SEED H B, IDRISS I M, MAKDISI F, et al. Representation of Irregular Stress Time Histories by Equivalent Uniform Stress Series in Liquefaction Analysis [M]. California: University of California, 1975.

[62] XU D S, TANG J Y, ZOU Y, et al. Macro and micro investigation of gravel content on simple shear behavior of sand-gravel mixture[J]. Construction and Building Materials, 2019, 221: 730-744.

[63] O' SULLIVAN C. Particulate Discrete Element Modelling [M]. London: CRC Press, 2011.

[64] XU H, WANG X Y, LIU C N, et al. A 3D root system morphological and mechanical model based on L-Systems and its application to estimate the shear strength of root-soil composites[J]. Soil and Tillage Research, 2021, 212: 105074.

[65] JIANG M J, ZHU Y G, XI B L. Investigation into the soil-root composites using distinct element method[C]//LI X K, FENG Y T, MUSTOE G. Proceedings of the 7th International Conference on Discrete Element Methods. Singapore: Springer, Singapore, 2017: 1075-1083.

[66] SUN Y, LI H, CHENG Z F, et al. Experimental and numerical simulation study on mechanical properties of shallow slope root-soil composite in Qinghai area[J]. KSCE Journal of Civil Engineering, 2023, 27(7): 2834-2852.

[67] WANG J, LIU F Y, WANG P, et al. Particle size effects on coarse soil-geogrid interface response in cyclic and post-cyclic direct shear tests[J]. Geotextiles and Geomembranes, 2016, 44(6): 854-861.

[68] NONG Z Z, PARK S S, JEONG S W, et al. Effect of cyclic loading frequency on liquefaction prediction of sand[J]. Applied Sciences, 2020, 10(13): 4502.

[69] NONG Z Z, PARK S S. Effect of loading frequency on volumetric strain accumulation and stiffness improvement in sand under drained cyclic direct simple shear tests[J]. Journal of Geotechnical and Geoenvironmental Engineering, 2021, 147(12): 04021159.

[70] TANG C S, SHI B, ZHAO L Z. Interfacial shear strength of fiber reinforced soil[J]. Geotextiles and Geomembranes, 2010, 28(1): 54-62.

[71] FAN C C, TSAI M H. Spatial distribution of plant root forces in root-permeated soils subject to shear[J]. Soil and Tillage Research, 2016, 156: 1-15.

[72] GENET M, STOKES A, SALIN F, et al. The influence of cellulose content on tensile strength in tree roots[J]. Plant and Soil, 2005, 278(1/2): 8768.

[73] THOMAS R E, POLLEN-BANKHEAD N. Modeling root-reinforcement with a fiber-bundle model and Monte Carlo simulation [J]. Ecological Engineering, 2009, 36(1): 47-61.

[74] WALDRON L J, DAKESSIAN S. Soil reinforcement by roots[J]. Soil Science, 1981, 132(6): 427-435.

[75] GHESTEM M, VEYLON G, BERNARD A, et al. Influence of plant root system morphology and architectural traits on soil shear resistance[J]. Plant and Soil, 2014, 377(1/2): 43-61.

[76] MASI E B, SEGONI S, TOFANI V. Root reinforcement in slope stability models: a review[J]. Geosciences, 2021, 11(5): 212.

[77] FAN C C. A displacement-based model for estimating the shear resistance of root-permeated soils[J]. Plant and Soil, 2012, 355(1/2): 103-119.

[78] JEWELL R A, WROTH C P. Direct shear tests on reinforced sand [J]. Geotechnique, 1987, 37(1): 53-68.

(责任编辑 王海锋)